

Bending relaxation of H₂O by collision with para- and ortho-H₂

Ricardo Manuel García-Vázquez ¹, Alexandre Faure ², Thierry Stoecklin ^{1,*}

¹UMR5255-CNRS, Université de Bordeaux, 351 cours de la libération, F-33405 Talence, France.

²Univ. Grenoble Alpes, CNRS, IPAG, F-38000 Grenoble, France.

*Correspondence: thierry.stoecklin@u-bordeaux.fr

ABSTRACT

We extend our recent theoretical work on the bending relaxation of H₂O in collisions with H₂ by including the three water modes of vibration coupled with rotation, as well as the rotation of H₂. Our full quantum close-coupling method (excluding the H₂ vibration) is combined with a high-accuracy nine-dimensional potential energy surface. The collisions of para-H₂O and ortho-H₂O with the two spin modifications of H₂ are considered and compared for several initial states of H₂O. The convergence of the results as a function of the size of the rotational basis set of the two colliders is discussed. In particular, near-resonant energy transfer between H₂O and H₂ is found to control the vibrational relaxation process, with a dominant contribution of transitions with $\Delta j_2 = j_2^i - j_2^f = +2, +4$, j_2^i and j_2^f being respectively the H₂ initial and final rotational quantum numbers. Finally, the calculated value of the H₂O bending relaxation rate coefficient at 295 K is found to be in excellent agreement with its experimental estimate.

INTRODUCTION

Until very recently, the modeling of molecular excitation in the interstellar medium only took into account the rotation of the molecules detected, due to the cold temperatures (< 100 K) prevailing in interstellar clouds. However, some of the most abundant triatomic interstellar molecules, such as HCN¹ and C₃², have been detected in highly excited vibrational states in warmer environments, e.g. in star-forming regions and in the envelopes of giant stars. The large quantity of water present in the Earth's atmosphere made it very difficult to detect H₂O in ro-vibrationally excited states but the construction of the Atacama Large Millimeter/submillimeter Array (ALMA) interferometer partially overcame these constraints and enabled the first measurements of water transitions into vibrationally excited states, up to $(v_1, v_2, v_3) = (0, 1, 1)$, as part of the Atomium project³. More recently, the launch of the James Webb Space Telescope (JWST) has not only freed us from the Earth's atmosphere, but has also widened the window of detection to vibrational wavelengths, with e.g. the very recent detection of water vapor in the terrestrial planet-forming region of a protoplanetary disk⁴.

Collisional rate coefficients of H₂ with water in vibrationally excited levels are then urgently needed by the astrochemists. On the theoretical side, the first quantum calculations dedicated to collisions involving vibrationally excited polyatomic molecules were performed by Dagdigian and Alexander in 2013⁵ for the umbrella modes of CH₃ colliding with He and by Loreau and Van der Avoird in 2015 for the umbrella modes of NH₃ in collisions with He⁶. We developed our own approach to treat the bending relaxation of a linear triatomic molecule colliding with an atom shortly after and applied it to the He-HCN^{7,8}, He-C₃⁹⁻¹¹ and He-DCN¹² collisions. This method uses the internal coordinates Hamiltonian developed by Handy and Tennyson¹³ restricted to its rigid bender form to compute the triatomic molecule ro-vibrational

bound state energies and wave functions. We extended this approach recently to collisions involving an atom and a non linear symmetric triatomic molecule and applied it to the bending relaxation of H₂O colliding with para-H₂¹⁴, para-H₂ being treated as fictitious atom. In 2021 the team of Guo used a very similar approach to treat the vibrational relaxation of water, including the bending and stretching modes, in collisions with Cl¹⁵ and Ar¹⁶. They used Radau coordinates instead of Bond length Bond angle coordinates to obtain the triatomic energies and wave functions. For many years the only calculations available regarding the H₂ + H₂O collision and taking into account the rotation of H₂ as well as the bending and rotation of H₂O were the Quasi-Classical Trajectory (QCT) calculations performed by Faure et al.¹⁷ using the full-dimensional (9D) potential energy surface (PES), fully described in Valiron et al.¹⁸. The first quantum calculations of the bending relaxation of water by collisions with H₂ taking into account the rotation of H₂ were performed by Wiesenfeld in 2021¹⁹. These calculations however did not include yet the coupling between the bending and rotation of H₂O. The object of the present study is then to extend our previous work on this system¹⁴ by taking also into account both the rotation of H₂ and the two stretching modes of H₂O. To this aim we use the same 9D PES developed by Valiron et al.¹⁸. The paper is organised as follows: In section [Method](#) the main elements of the method are briefly reminded and the modifications necessary to perform the dynamics calculations are discussed. In section [Calculations and results](#) the results are presented and the bending relaxation rate coefficient is compared to the experimental data available. In section [Conclusion](#) a few conclusions are given.

METHOD

The rigid rotor Close Coupling equations for the collisions of H₂ + H₂O were given long ago in detail by Phillips et al.²⁰ and we refer the interested reader to this paper. The extension of the theory to vibrating molecules is straightforward and only a brief account of the main steps of the calculations will be given in section [Close Coupling equations](#). The Schrödinger equation of the system is expressed in the (X', Y', Z') Space fixed frame which is obtained by a simple rotation of the inertial H₂O (X, Y, Z) frame illustrated in Fig. 1 where \vec{R} is the intermolecular vector between the centers of mass of H₂O and H₂ and (R, θ_R , φ_R) are its spherical coordinates in this frame where the relative interaction potential briefly described in the following section is also computed. As can be seen on this figure the water molecule is lying in the XOZ molecular plane while the C₂ Z axis is bisecting the bending angle.

Potential energy surface

We use an 8D restriction to non vibrating H₂ of the 9D PES of Valiron et al.¹⁸ which is expanded in the rigid rotor Green's angular basis set²¹

$$t_{p_1 p_2 p}^{q_1}(\theta_2, \varphi_2, \theta_R, \varphi_R) = \frac{\alpha_{p_1 p_2 p}^{q_1}}{(1 + \delta_{q_1 r_1})} \sum_{r_1, r_2} \begin{pmatrix} p_1 & p_2 & p \\ r_1 & r_2 & r \end{pmatrix} \times Y_{p_2}^{r_2}(\theta_2, \varphi_2) Y_p^r(\theta_R, \varphi_R) [\delta_{q_1 r_1} + (-1)^{(p_1 + q_1 + p_2 + p)} \delta_{-q_1 r_1}] \quad (1)$$

for each value of the H₂O Radau coordinates (R₁, R₂, α) and the intermolecular distance R:

$$V(R_1, R_2, \alpha, R, \theta_2, \varphi_2, \theta_R, \varphi_R) = \sum_{p_1 q_1 p_2 p} V_{p_1 p_2 p}^{q_1}(R_1, R_2, \alpha, R) t_{p_1 p_2 p}^{q_1}(\theta_2, \varphi_2, \theta_R, \varphi_R). \quad (2)$$

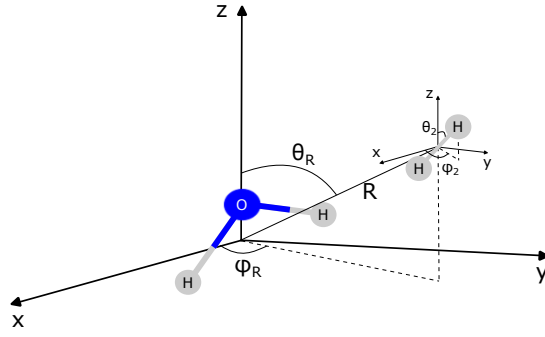


Figure 1: Coordinates used for the H₂-H₂O collision. The water molecule lies in the XOZ plane where O the H₂O center of mass and the Z axis is bisecting the bending angle.

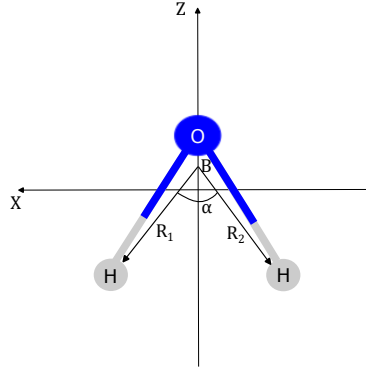


Figure 2: Coordinates used for the calculation of the H₂O bound states. B is the Radau canonical point of H₂O, R₁ and R₂ are the modulus of the vectors that defines the position of the two hydrogen atoms with respect to the B point and α is the angle between these two vectors.

In Eq. (1), the normalization factor is¹⁸:

$$\alpha_{p_1 p_2 p}^{q_1} = [2(1 + \delta_{q_1 0})^{-1} (2p_1 + 1)^{-1}]^{-1/2}. \quad (3)$$

Calculations of the ro-vibrational bound states of H₂O

Many papers have been devoted to the study of Energy levels and spectra of the water molecule from the experimental and theoretical point of view. Very accurate results can be found, for example, in Ref. 22,23, and we encourage the people interested in the use of an extensive list of energy levels to refer to these papers. The first objective of this section is the determination of the H₂O rovibrational wave functions which will be used for performing the dynamics calculations. The second objective is to point out the main differences between our new approach and the one used in our previous work on the system¹⁴ as well as with the widely used DVR3D method¹³.

In our previous work dedicated to the rigid bender inelastic collision of H₂O colliding with para-H₂¹⁴ we used bond length bond angle coordinates together with the Hamiltonian of Tennyson and Sutcliffe²⁴ to describe the internal motion of the water molecule. The rigid bender Hamiltonian equations were solved in the X bisector embedding frame and the solutions rotated in the X-Z plane by an angle of $\frac{\pi}{2}$ in order to perform the dynamics .

In the present work, as we need to describe equally the stretching, bending and rotation of H₂O, we use instead Radau

coordinates (R_1, R_2, α) (see Fig. 2) and the Z bisector embedding. This choice simplifies the hamiltonian by cancelling the radial cross derivatives that appears in the bond length bond angle Hamiltonian and also eliminating the need of the rotation step after diagonalization. It furthermore offers an excellent compromise of accuracy and computer time to calculate the H₂O ro-vibrational bound states energies and wave functions as demonstrated by Tennyson¹³. In what follows we give the details of our implementation of the method for solving these equations as it differs in several respects from the approach used in the code DVR3D¹³ like for example using Potential Optimised Discrete Variable Representation (PODVR)^{15,25}.

The H₂O Hamiltonian takes the following form in Radau coordinates (R_1, R_2, α) and atomic units²⁶:

$$\hat{H}_{ABC} = -\frac{1}{2\mu_1} \frac{\partial^2}{\partial R_1^2} - \frac{1}{2\mu_2} \frac{\partial^2}{\partial R_2^2} + \hat{T}_\alpha + \hat{T}_{vr} + V_{ABC}(R_1, R_2, \alpha) \quad (4)$$

where \hat{T}_α and \hat{T}_{vr} are respectively the kinetic operators associated with the Radau angle α and with the coupling between vibration and rotation as defined in Ref. [26] while the μ_i are the reduced masses associated with the R_i coordinates¹³. The expression (4) is as usual re-written in terms of single radial coordinate hamiltonian of R_1 and R_2 as:

$$\hat{H}_{ABC} = \hat{h}_1(R_1) + \hat{h}_2(R_2) + \hat{T}_\alpha + \hat{T}_{vr} + \hat{V}_{res}(R_1, R_2, \alpha) \quad (5)$$

where $\hat{h}_i, i = 1, 2$ are defined as:

$$\hat{h}_i(R_i) = -\frac{1}{2\mu_i} \frac{\partial^2}{\partial R_i^2} + \hat{V}_i(R_i) \quad (6)$$

These reference hamiltonians are similar to those used in Ref. [15] with the difference that we use the reduced masses μ_1 and μ_2 instead of the atomic masses m_A and m_C . The $\hat{V}_i(R_i)$ and $\hat{V}_{res}(R_1, R_2, \alpha)$ potentials are defined in the same way as in Ref. [15]:

$$\hat{V}_1(R_1) = \hat{V}_{ABC}(R_1, R_2^e, \alpha^e) \quad (7)$$

$$\hat{V}_2(R_2) = \hat{V}_{ABC}(R_1^e, R_2, \alpha^e) \quad (8)$$

$$\hat{V}_{res}(R_1, R_2, \alpha) = \hat{V}_{ABC}(R_1, R_2, \alpha) - \hat{V}_1(R_1) - \hat{V}_2(R_2) \quad (9)$$

where (R_1^e, R_2^e, α^e) are the values of the Radau coordinates for the equilibrium geometry of the ABC molecule.

For the sake of simplicity the H₂O rotational angular momentum j_1 as well as its space fixed Z axis projection m_{j_1} will be denoted only j and m_j in the present section. The general basis set describing both the vibration and rotation of the triatomic molecule is written:

$$|n_1 n_2 n j \bar{k} m_j, p\rangle = |n_1\rangle |n_2\rangle |n j \bar{k} m_j, p\rangle. \quad (10)$$

where $|n j \bar{k} m_j, p\rangle$ is the symmetrized rovibrational basis set describing the bending and rotation part as defined by Sutcliffe and Tennyson²⁷ and also used in our previous work¹⁴ :

$$|jn\bar{k}m_j, p\rangle = \frac{1}{\sqrt{2(1 + \delta_{\bar{k},0})}} [|jn\bar{k}m_j\rangle + (-1)^p |jn - \bar{k}m_j\rangle] \quad (11)$$

with

$$|jn\bar{k}m_j\rangle = P_n^{\bar{k}}(\cos\alpha) |j\bar{k}m_j\rangle \quad (12)$$

where m_j and \bar{k} are the projections of the H₂O rotational angular momentum j along the z' space fixed and z molecular fixed axis respectively. $P_n^{\bar{k}}(\cos\alpha)$ is a generalized Legendre function while $|j\bar{k}m_j\rangle$ is a symmetric top wave function. $|n_1\rangle$ and $|n_2\rangle$ are the eigenvectors of the radial reference Hamiltonians $\hat{h}_i, i = 1, 2$ in a PODVR approach^{15,25}:

$$\hat{h}_i |n_i\rangle = \epsilon_{n_i}^i |n_i\rangle, i = 1, 2. \quad (13)$$

We use a Gauss-Lanczos-Morse-DVR (GLM-DVR) basis²⁸ as a primitive basis for the PODVR, instead of the usual sine-DVR basis considered for example in Ref.[15] as it describes better the anharmonicity of the radial reference potentials. The resulting irregular radial grid gives a very good accuracy for a reduced number of points.

For A₂B molecules one may furthermore take advantage of the permutation symmetry and use a symmetrized radial basis:

$$|n_1 n_2, q\rangle = N_{n_1, n_2} [|n_1 n_2\rangle + (-1)^{q+\bar{k}} |n_2 n_1\rangle] \quad (14)$$

with $N_{n_1, n_2} = \frac{1}{\sqrt{2(1 + \delta_{n_1, n_2})}}$, $n_1 \geq n_2$ for $q + \bar{k}$ even and $n_1 > n_2$ for $q + \bar{k}$ odd¹³. This expression, as discussed in Tenynson et al.¹³, presents the great advantage to allow selecting ortho and para symmetry blocks of A₂B molecules by choosing a value of q . In the case of water $q = 0$ and $q = 1$ are respectively associated with the para and ortho symmetries.

From the matrix elements of the triatomic hamiltonian in the unsymmetrized basis set reported in Refs.[26,29] one can easily derive the non-zero matrix elements in the symmetrized basis:

$$\langle n_1 n_2 n j \bar{k} m_j, q, p | \hat{h}_1 + \hat{h}_2 | n'_1 n'_2 n j \bar{k} m_j, q, p \rangle = 2N_{n_1, n_2} N_{n'_1, n'_2} (\epsilon_{n_1} + \epsilon_{n_2}) [\delta_{n_1, n'_1} \delta_{n_2, n'_2} + (-1)^{q+\bar{k}} \delta_{n_1, n'_2} \delta_{n_2, n'_1}] \quad (15)$$

$$\langle n_1 n_2 n j \bar{k} m_j, q, p | \hat{T}_\alpha + \hat{T}_{vr} | n'_1 n'_2 n' j \bar{k} m_j, q, p \rangle = M_{n_1, n_2, n'_1, n'_2, q, \bar{k}} \times \left\{ \frac{1}{8} [j(j+1) - \bar{k}^2] \delta_{n, n'} + n(n+1) \delta_{n, n'} + \frac{1}{4} [j(j+1) - 3\bar{k}^2] E_{n, n', \bar{k}} \right\} \quad (16)$$

$$\begin{aligned} \langle n_1 n_2 n j \bar{k} m_j, q, p | \hat{T}_\alpha + \hat{T}_{vr} | n'_1 n'_2 n' j \bar{k} \pm 1 m_j, q, p \rangle &= \frac{1}{4} (1 + \delta_{\bar{k}, 0})^{\frac{1}{2}} (1 + \delta_{\bar{k} \pm 1, 0})^{\frac{1}{2}} \lambda_{j\bar{k}}^\pm R_{n_1, n_2, n'_1, n'_2, q, \bar{k}} \\ &\times \left\{ (2\bar{k} + 1)(G_{n, n', \bar{k}} - D_{n, n', \bar{k}}) - 2\lambda_{n, \bar{k}}^\pm \delta_{n, n'} \right\} \end{aligned} \quad (17)$$

$$\langle n_1 n_2 n j \bar{k} m_j, q, p | \hat{T}_\alpha + \hat{T}_{vr} | n'_1 n'_2 n' j \bar{k} \pm 2 m_j, q, p \rangle = \frac{1}{16} (1 + \delta_{\bar{k},0})^{\frac{1}{2}} (1 + \delta_{\bar{k} \pm 2,0})^{\frac{1}{2}} \lambda_{j\bar{k}}^\pm \lambda_{j\bar{k} \pm 1}^\pm \times M_{n_1, n_2, n'_1, n'_2, q, \bar{k}} \times (2F_{n, n', \bar{k}} - H_{n, n', \bar{k}}) \quad (18)$$

with $\lambda_{lm}^\pm = \sqrt{l(l+1) - m(m \pm 1)}$ and:

$$M_{n_1, n_2, n'_1, n'_2, q, \bar{k}} = 2N_{n_1, n_2} N_{n'_1, n'_2} \times [A_{n_1, n_2, n'_1, n'_2} + (-1)^{q+\bar{k}} A_{n_1, n_2, n'_2, n'_1}], \quad (19)$$

$$R_{n_1, n_2, n'_1, n'_2, q, \bar{k}} = 2N_{n_1, n_2} N_{n'_1, n'_2} \times [B_{n_1, n_2, n'_1, n'_2} + (-1)^{q+\bar{k}} B_{n_1, n_2, n'_2, n'_1}], \quad (20)$$

$$A_{n_1, n_2, n'_1, n'_2} = \langle n_1 n_2 | \frac{1}{2\mu_1 R_1^2} + \frac{1}{2\mu_2 R_2^2} | n'_1 n'_2 \rangle, \quad (21)$$

$$B_{n_1, n_2, n'_1, n'_2} = \langle n_1 n_2 | \frac{1}{2\mu_1 R_1^2} - \frac{1}{2\mu_2 R_2^2} | n'_1 n'_2 \rangle. \quad (22)$$

where the $E_{n, n', \bar{k}}$, $G_{n, n', \bar{k}}$, $D_{n, n', \bar{k}}$, $F_{n, n', \bar{k}}$ and $H_{n, n', \bar{k}}$ are angular integrals defined in Ref.[26] which are computed using a Gauss-Legendre quadrature. For $\bar{k} = \bar{k}' = 1$ there is an extra term in the symmetrized hamiltonian coming from the $\bar{k} \pm 2, \bar{k}$ elements when $\bar{k}' = -1$ and $\bar{k} = 1$ in the unsymmetrized basis. This extra terms is defined as:

$$\langle n_1 n_2 n j (\bar{k} = 1) m_j, q, p | \hat{T}_\alpha + \hat{T}_{vr} | n'_1 n'_2 n' j (\bar{k} = 1) m_j, q, p \rangle = \frac{(-1)^{1-p}}{16} j(j+1) M_{n_1, n_2, n'_1, n'_2, q, \bar{k}} \times (2F_{n, n', \bar{k}} - H_{n, n', \bar{k}}) \quad (23)$$

The symmetrised integrals over the potential take the following form:

$$\langle n_1 n_2 n j \bar{k} m_j, q, p | V_{res}(R_1, R_2, \alpha) | n'_1 n'_2 n' j \bar{k} m_j, q, p \rangle = 2N_{n_1, n_2} N_{n'_1, n'_2} \times [\langle n_1 n_2 n j \bar{k} m_j | V_{res}(R_1, R_2, \alpha) | n'_1 n'_2 n' j \bar{k} m_j \rangle + (-1)^{q+\bar{k}} \langle n_1 n_2 n j \bar{k} m_j | V_{res}(R_1, R_2, \alpha) | n'_2 n'_1 n' j \bar{k} m_j \rangle] \quad (24)$$

They are computed using a Gauss-Legendre quadrature for the integration over the Radau bending angle (α) and a GLM-PODVR quadrature over the radial Radau coordinates.

Close Coupling equations

We follow closely the approach detailed in the original paper of Phillips et al.²⁰ dedicated to the rigid rotor approach of the H_2-H_2O collisions where the reader can find the details of the derivation. We here only give their slightly modified form in order to refer to the three modes of vibration of the H_2O molecule which can be coupled by the intermolecular potential. We do not include the H_2 vibration in our notation as it is neglected in the present approach. We will for rotation refer to the angular momenta \vec{j}_1 , \vec{j}_2 and \vec{T} associated respectively with H_2O , H_2 and their relative angular mo-

mentum while $\vec{j}_{12} = \vec{j}_1 + \vec{j}_2$ and the τ index allows distinguishing the H₂O rotational states inside a given j_1 multiplet. In order to further simplify the notations we will use the collective index (i) to designate the set of quantum numbers $(v_1 v_2 v_3 j_1 \tau j_2)$ associated with a given internal state of the H₂-H₂O complex, where $(v_1 v_2 v_3)$ are the vibrational quantum numbers for, respectively, the symmetry stretching, the bending, and the antisymmetric stretching of H₂O. The close-coupling equations for the radial part of the scattering wave function read:

$$\left\{ \frac{d^2}{dR^2} - \frac{l(l+1)}{R^2} + k_{(i)}^2 \delta_{(i),(j)} \delta_{j_{12} j'_{12}} \delta_{l l'} - [U(R)]_{(i)j_{12}l;(j)j'_{12}l'}^{JMP} \right\} \times G_{(i)j_{12}l;(j)j'_{12}l'}^{JMP}(R) = 0 \quad (25)$$

where $G_{(i)j_{12}l;(j)j'_{12}l'}^{JMP}(R)$ is the radial part of the H₂-H₂O scattering wave function, $k_{(i)}^2 = 2\mu[E - \varepsilon_{(i)}]$ and

$$[U(R)]_{(i)j_{12}l;(j)j'_{12}l'}^{JMP} = 2\mu \sum_{p_1 q_1 p_2 p} \langle (i)j_{12}l JM | t_{p_1 p_2 p}^{q_1} | (j)j'_{12}l' JM \rangle \times \int_0^\pi d\alpha \sin(\alpha) \int dR_1 \int dR_2 [\Gamma_{v_1 v_2 v_3}^{j_1 \tau}(R_1, R_2, \alpha) \times V_{p_1 p_2 p}^{q_1}(R_1, R_2, \alpha, R) \times \Gamma_{v'_1 v'_2 v'_3}^{j'_1 \tau'}(R_1, R_2, \alpha)] \quad (26)$$

In this expression the $\Gamma_{v_1 v_2 v_3}^{j_1 \tau}(R_1, R_2, \alpha)$ are the H₂O wave functions calculated in the previous section while the $\langle (i)j_{12}l JM | t_{p_1 p_2 p}^{q_1} | (j)j'_{12}l' JM \rangle$ are the rigid rotor analytical angular matrix elements of the potential given in the paper of Phillips et al.²⁰. J and M are respectively the total angular momentum and its projection along the Z space fixed axis while P is the parity of the system. We furthermore replace the $\varepsilon_{(i)}$ calculated in the previous section by their experimental values.

A new code called `Divitas` and including many of the ingredients of the `Newmat`³⁰ and `Didimat`³¹ code was written in Bordeaux. It includes the calculations of the ro-vibrational states of H₂O detailed in section Calculations of the ro-vibrational bound states of H₂O and solves the space fixed Close Coupling equations (25) using a log derivative propagator³². It was tested by reproducing the rigid rotor calculations performed in Grenoble using the `Molscat` code³³.

CALCULATIONS AND RESULTS

H₂O bound states

We use the most recent POKAZATEL PES of water²³ to compute the energy levels of the water molecule for 8 values of the rotational state $j_1 = 0 - 7$. This PES which is the most accurate available was specifically designed to describe very excited ro-vibrational H₂O states. Our basis set contains 4 GLM-PODVR functions for each R_1 and R_2 radial coordinates and 45 values of n . Angular integrals were computed using 50 Gauss-Legendre quadrature points while the radial integrals use a two dimensional R_1, R_2 grid of 10 GLM-PODVR points for $q + \bar{k}$ even and 6 points for $q + \bar{k}$ odd due to the use of radial symmetrized basis.

The GLM-PODVR basis set is eigenfunction of the 1D reference hamiltonian \hat{h}_1 (due to the symmetry of the water molecule \hat{h}_1 and \hat{h}_2 are identical) and is obtained using a 100 point 1D GLM-DVR spanning the $[0.9, 4.5] a_o$ interval. A grid of 30 points is enough to achieve a convergence better than 0.3 cm^{-1} for all the calculated states and better than 0.01 cm^{-1} if we consider only the rotational states inside the $(0, 0, 0)$, $(0, 1, 0)$ and $(0, 2, 0)$ vibrational states.

(v_1, v_2, v_3)	(EXP-TW)	(EXP-TW2)	(EXP-POL)
(0,1,0)	0.374	0.158	-0.310
(0,2,0)	0.727	0.484	-0.540
(1,0,0)	0.840	-0.242	-0.840
(0,0,1)	0.838	-0.039	-0.730

Table 1: Comparison between theory and experiment of the 4 first excited vibrational energy levels of H₂O ($j = 0$) calculated using our approach and the POKAZATEL PES²³ (TW) or the PES reported in Ref 22 (TW2). The errors reported in Ref 22 (POL) using DVR3D are reported in the last column. Units are cm⁻¹.

(v_1, v_2, v_3)	j_{kac}	EXP	(EXP-YA)	(EXP-TW)	(v_1, v_2, v_3)	j_{kac}	EXP	(EXP-YA)	(EXP-TW)
para-H ₂ O					ortho-H ₂ O				
(0,0,0)	0 ₀₀	0	0	0	(0,0,0)	1 ₀₁	23.794	0.094	-0.016
(0,1,0)	0 ₀₀	1594.746	-0.754	0.374	(0,1,0)	1 ₀₁	1618.557	-0.643	0.302
(0,2,0)	0 ₀₀	3151.630	-2.170	0.727	(0,2,0)	1 ₀₁	3175.441	-2.159	0.598
(1,0,0)	0 ₀₀	3657.053	9.253	0.840	(1,0,0)	1 ₀₁	3680.454	9.354	0.877
	1 ₁₁	3693.294	9.494	0.857		1 ₁₀	3698.491	9.491	0.957
	2 ₀₂	3725.942	9.442	0.920		2 ₁₂	3734.897	9.597	0.837
	2 ₁₁	3750.465	9.565	0.934		2 ₂₁	3788.694	10.094	1.079
	2 ₂₀	3789.969	10.069	0.882		3 ₀₃	3791.372	9.672	0.887
	3 ₁₃	3796.540	9.740	0.980		3 ₁₂	3827.393	9.793	1.134
	4 ₂₂	3966.559	10.359	0.911		3 ₂₁	3864.764	10.164	0.961
	5 ₃₃	4150.287	11.487	1.388		3 ₃₀	3935.345	11.045	1.014
(0,0,1)	1 ₀₁	3779.493	11.193	0.783	(0,0,1)	0 ₀₀	3755.928	11.128	0.838
	3 ₁₂	3926.862	11.662	1.218		3 ₂₂	3956.666	12.066	1.337

Table 2: Comparison of the experimental energy levels of para- and ortho-H₂O (EXP) with the theoretical results reported in Yang et al.³⁴ (YA) and the ones obtained in this work (TW). The experimental values as well as the absolute errors are reported in cm⁻¹.

The comparison with experiment shows the very good accuracy achieved in the present calculations. For all the 320 ro-vibrational states computed in the present work, the maximum percentage error was 0.222 % for para states and 0.218 % for the ortho ones.

Very accurate H₂O ro-vibrational bound state energies were reported by POKAZATEL²³. These authors used the parametrised POKAZATEL PES²³ that was calculated from ab initio points and fitted to the experimental energy values with the help of the DVR3D package¹³. This semi empirical PES error leads to a very good accuracy of the bound state energies which is better than 0.05 cm⁻¹ provided that the DVR3D method is used for the bound states calculations as it was used to perform the fit. As our PES is not fitted on experiment, we compare our results with other non-semi-empirical values provided by the same authors using just an ab initio PES²². We present in Table 1 the results of this comparison and observe their excellent agreement. We furthermore can see that our most accurate results are obtained from the PES of Ref. 22 which is not semi empirical. We then conclude that the use of the ab initio + semi-empirical PES²³ leads to better results only if the DVR3D method which was used to perform the fit is also used to calculate the levels. A comparison with the rovibrational states recently computed by Yang et al.³⁴ using their ab initio PES is also presented in Table 2. The present approach appears to be more accurate by about a factor of ten.

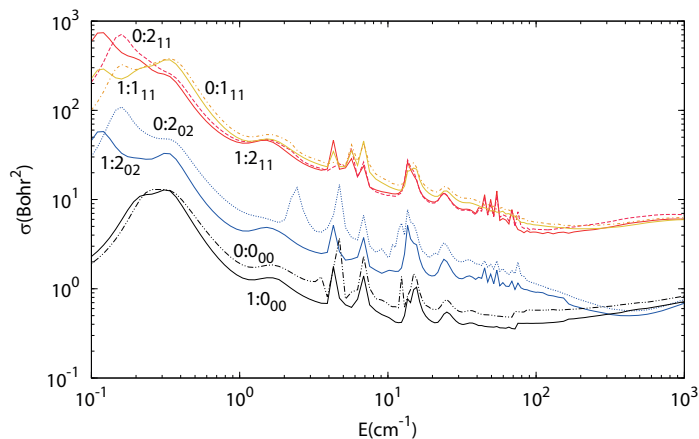


Figure 3: Comparison between rotationally inelastic state to state cross section for $\text{H}_2\text{O}(v_2, 2_{20})$ colliding with para- $\text{H}_2(j = 0)$ inside $v_2 = 0$ and 1. The final H_2O ro-vibrational state is indicated on each curve. The solid and dashed line are respectively associated with transitions inside $v_2 = 1$ and 0.

Close-Coupling calculations

As mentioned in section the new code is an extension of the `Newmat` code version which was recently developed for treating the bending relaxation of H_2O colliding with an atom¹⁴. It was then tested by reproducing calculations performed in recent work for the bending relaxation of H_2O by collisions with He³⁵. It was also tested by reproducing Molscat rigid rotor calculations for the $\text{H}_2 + \text{H}_2\text{O}$ collisions³⁶ using the experimental values of the H_2 rotational constants³⁷. For all the calculations presented, three levels of each H_2 spin modification were necessary to converge the bending relaxation cross section. Rotational states of H_2O for $j_1=0$ to 5 were included in the two bending states considered in the calculations. This choice of basis resulting from a compromise between computer time and accuracy allowed us to include the $j = 5$ level of H_2 which was neglected in previous calculations³⁸. We checked that increasing the rotational basis set of H_2O up to $j=7$ only marginally affects the magnitude of the bending relaxation cross section for levels with $j \leq 5$. A Chebyshev grid of 18 bending angles and the same two dimensional R_1, R_2 GLM-PODVR grid used before for the calculation of the wave functions of H_2O was used to calculate the vibrational part of the potential matrix elements while 20 closed channels were included for each collision energy in the $0.1\text{-}1000 \text{ cm}^{-1}$ interval. This is corresponding to a maximum rotational energy of about 4200 cm^{-1} , which is slightly higher than the 3500 cm^{-1} used by Wiesenfeld¹⁹. Relative convergence of the bending relaxation cross section was tested as a function of the total angular momentum J for each collision energy to be better than 10^{-6} leading to a maximum value of $J = 65$ at 1000 cm^{-1} , which is more than the double of the maximum value of $J = 32$ used by Wiesenfeld³⁸.

Rotational transitions inside a given bending level of H_2O

We compare in Figure 3 pure rotational transitions inside $v_2 = 0$ and 1 and starting from the 2_{20} level of H_2O in collision with para- $\text{H}_2(j_2 = 0)$. The final state of H_2 is ($j_2 = 0$) for all the H_2O transitions represented. As can be seen on this figure the position of the resonances are about the same for the transitions considered inside the two different bending levels. The magnitudes are conversely seen to be slightly lower in the excited $v_2 = 1$ level. This is not surprising as channels associated with excited levels of H_2 (for example $j_2=4 + \text{H}_2\text{O}(v_2 = 0, 5_{24})$) are open and interspersed

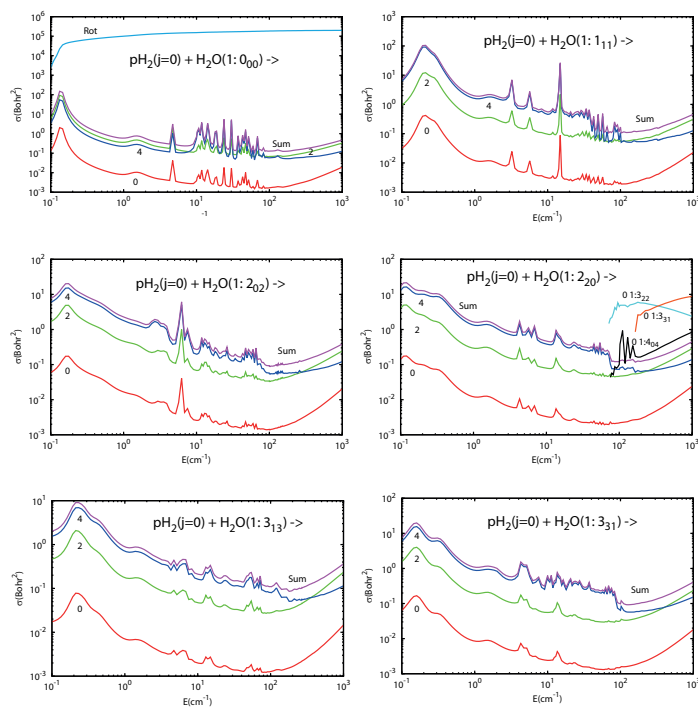


Figure 4: Comparison between the vibrational quenching cross section of para- $\text{H}_2\text{O}(v_2 = 1, j_{k_a k_c})$ by collision with para- $\text{H}_2(j = 0)$ for several initial levels of H_2O belonging to the $v_2 = 1, j = 0, 1, 2$ and 3 manifolds. The curves $0, 2, 4$ correspond to the final state of H_2 . In the middle right panel the opening of excited state of H_2O is shown. The first reported quantum number on these curves is denoting the rotation of H_2 while the others give the H_2O ro-vibrational state. In light blue (upper left panel) the summed rotationally inelastic cross section inside the initial $v_2 = 1$ level is also represented for comparison.

between open $v_2 = 1$ levels. This means that part of the scattering flux is directed to this open levels, lowering the magnitude of the cross sections obtained for the same transition inside the $v_2 = 0$ bending level.

Bending relaxation propensity rules

Impact of the initial and final H_2 rotational basis: Figures 4, 5, 6, 7 show the bending relaxation cross sections for the four combinations of spin modifications of H_2 and H_2O respectively p- $\text{H}_2 + \text{p-}\text{H}_2\text{O}$; p- $\text{H}_2 + \text{o-}\text{H}_2\text{O}$; o- $\text{H}_2 + \text{p-}\text{H}_2\text{O}$ and o- $\text{H}_2 + \text{o-}\text{H}_2\text{O}$. On each of this figure the contributions of the three rotational levels of H_2 considered in the calculations are reported as well as the total bending relaxation cross sections, again summed over the final states of water. If we consider first Figures 4 and 5 associated both with collisions of p- H_2 we see that the three $j_2 = 0, 2$ and 4 final channels are open and give (except for the initial level p- $\text{H}_2(j_2=0) + \text{H}_2\text{O}(1:0_{00})$) contributions in ascending order, the global bending relaxation cross section being always almost equal to the $j_2 = 4$ contribution, except above $\sim 200 - 300 \text{ cm}^{-1}$. This is in contrast with rotational relaxation which favours the lowest Δj . As a matter of fact vibrational relaxation is conversely controlled by a near-resonant energy transfer mechanism which means that the largest contributions to the bending relaxation cross sections are provided by the internal levels of the complex which are the closest in energy with the initial level. Pure rotational transitions inside the excited bending level of H_2O give cross sections increasing with collision energy and up to five orders of magnitude larger than the bending relaxation cross sections, as illustrated in the upper left panel of Figure 4. This results in the steps observed in the bending relaxation cross sections around 70 cm^{-1} associated with the opening of rotational levels inside the $v_2 = 1$ excited bending level

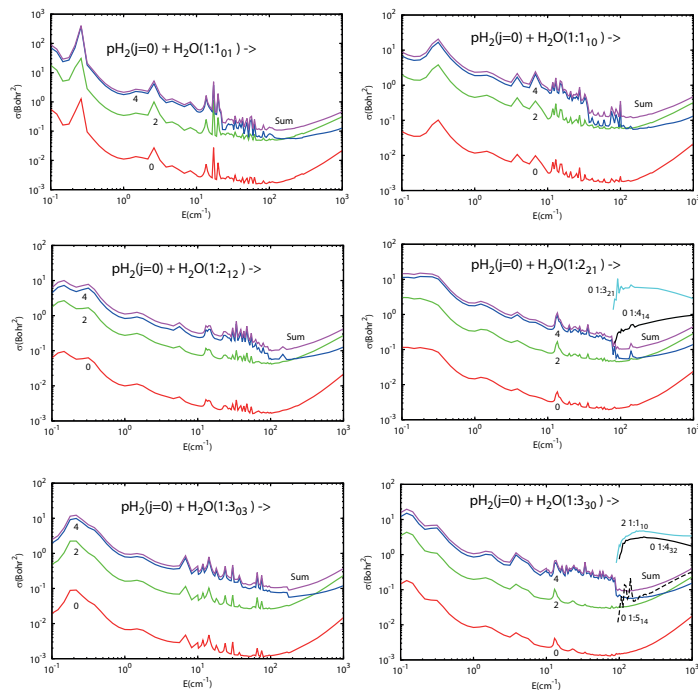


Figure 5: Comparison between the vibrational quenching cross section of ortho- $\text{H}_2\text{O}(v_2 = 1, j_{k_A k_C})$ by collision with para- $\text{H}_2(j = 0)$ for several initial levels of H_2O belonging to the $v_2 = 1, j = 1, 2$ and 3 manifolds. In the lower and middle right panels the opening of excited states (higher in energy than the initial state) of H_2O is also shown. The first reported quantum number on these curves is denoting the rotation of H_2 while the others give the H_2O ro-vibrational state.

of H_2O , as shown in the middle right panel of figure 4 and in the right middle and lower panels of figure 5 respectively for the opening of for example the p- $\text{H}_2(j=0) + \text{H}_2\text{O}(v_2 = 1, 3_{22})$ and p- $\text{H}_2(j=0) + \text{H}_2\text{O}(v_2 = 1, 3_{21})$ resulting in a decrease of the bending relaxation cross sections.

The strong dependence of the bending relaxation cross section as a function of the size of the H_2 rotational basis set included in the calculation explains why our first estimate of the bending relaxation cross section which considered only the $j = 0$ state of H_2 was two orders of magnitude smaller than the experimental value at 300 K, as suggested in that work¹⁴.

If we now compare Figures 6 and 7 associated both with collisions of o- H_2 we see that the final level $j_2 = 5$ is closed at low collision energy for many initial channels. This results in the main contribution to the bending relaxation cross section to be due to the $j_2 = 3$ final level for almost all the initial levels represented. The contribution of the $j_2 = 5$ final level is furthermore seen to exhibit many resonances as it is the closest in energy with the initial level and consequently the most sensitive to the opening of rotational levels inside the $v_2 = 1$ level of H_2O .

This important difference between the collisions of p- H_2 and o- H_2 analysed in the previous paragraph results in dramatic differences between the magnitude of the bending relaxation of H_2O at moderate collision energy specially for the lowest rotational state of the excited $v_2 = 1$ bending state. If we for example examine the case of the collisions of the p- $\text{H}_2\text{O}(v_2 = 1, 0_{00})$ state we see that the rotational state closer in energy in the $v_2 = 0$ manifold is the p- $\text{H}_2(j_2=4) + \text{H}_2\text{O}(v_2 = 0, 4_{31})$ in the case of the collisions with p- H_2 which is only about 24.5 cm^{-1} lower in energy than the initial state. In the case of the collisions with o- H_2 it is the o- $\text{H}_2(j_2=3) + \text{p-}\text{H}_2\text{O}(v_2 = 0, 5_{51})$ state which is about 259.5 cm^{-1}

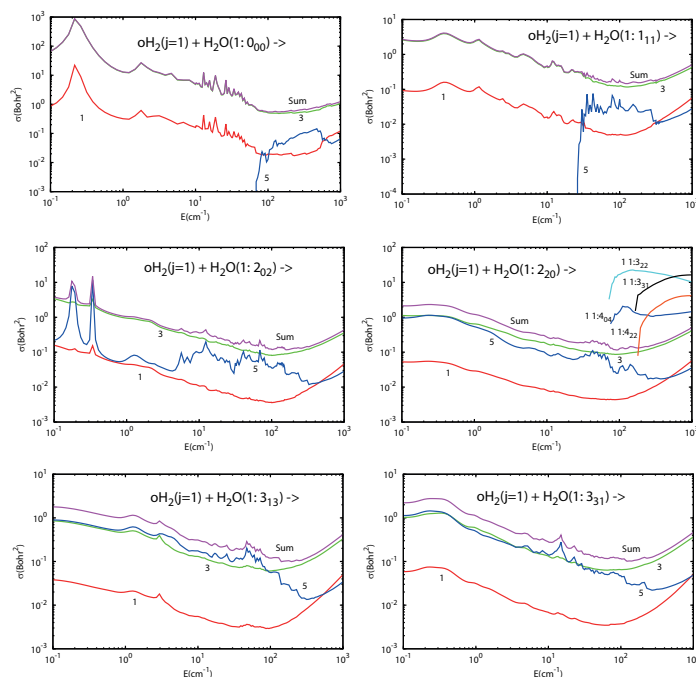


Figure 6: Comparison between the vibrational quenching cross section of para- $\text{H}_2\text{O}(v_2 = 1, j_{KA}k_C)$ by collision with ortho- $\text{H}_2(j = 1)$ for several initial levels of H_2O belonging to the $v_2 = 1, j = 0, 1, 2$ and 3 manifolds. The curves 1, 3, 5 correspond to the final state of H_2 . In the middle right panel, state to state cross sections associated with the opening of a few excited levels (higher in energy than the initial state) of H_2O are also represented. The first reported quantum number on these curves is denoting the rotation of H_2 while the others give the H_2O ro-vibrational state.

lower in energy than the initial state. As bending relaxation is controlled by a near-resonant energy transfer mechanism this means that bending relaxation of water is stronger with p- $\text{H}_2(j_2 = 0)$ than with o- $\text{H}_2(j_2 = 1)$ for moderate collision energies corresponding to the region of the potential well which is 235 cm^{-1} deep. There is, conversely, no visible tendency to favour either the ortho or the para transitions of H_2O for collisions with the same symmetry of H_2 (o- or p- H_2) as already noticed for the quenching of H_2O by atoms.³⁵

Impact of the initial H_2O rotational basis : $j(\text{H}_2\text{O})$ -selected vibrational quenching rate coefficient of a given ($v_2 = 1, j$) state of H_2O are compared for the collisions with the two spin modifications of H_2 in their ground state in Figure 8. They were obtained by Boltzmann averaging all the asymmetric top multiplet contributions (i.e. for each j) in the temperature range $0.5 - 500 \text{ K}$ and by using the ortho:para statistical weight $3:1$ for the water molecule. The global rate coefficient obtained by Boltzmann averaging the $j = 0 - 3$ selected rates is also represented.

In the limit of low collision energies, the $\text{H}_2\text{O}(j = 0)$ vibrational quenching rate is seen to be increasing as a function of collision energy for the collisions with o- H_2 while it decreases as collision energy increases for collisions with p- H_2 . We note that at higher temperatures (above 1500 K) which were not explored in the present approach, a rotational enhancement of the vibrational relaxation process was observed at the classical level for low j by Faure et al.⁴⁰. We indeed can already see for the collisions with both p- and o- H_2 that the $j = 1$ state selected quenching rate becomes larger than the one of $j = 0$ at higher temperature.

We note that for astrophysical applications, the most extensive collisional dataset for $\text{H}_2\text{O} + \text{H}_2$ is currently that of

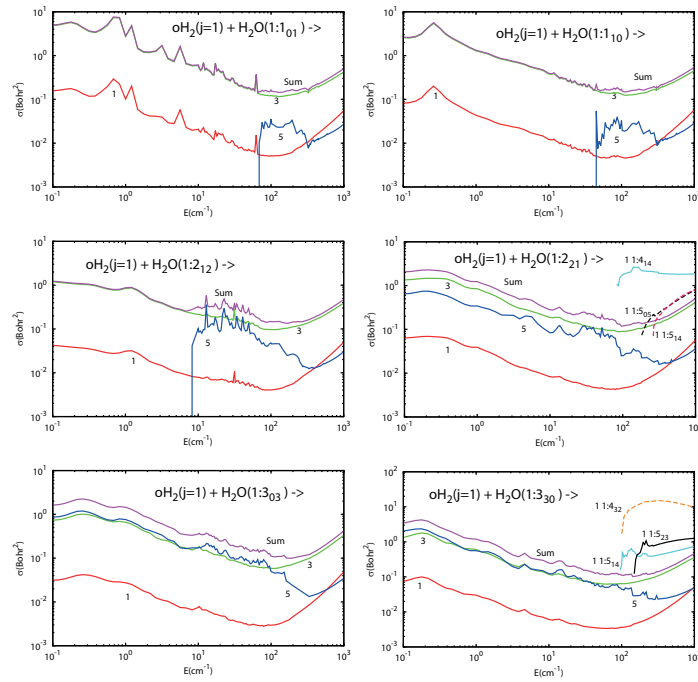


Figure 7: Comparison between the vibrational quenching cross section of ortho- $\text{H}_2\text{O}(v_2 = 1, j_{k_A k_C})$ by collision with ortho- $\text{H}_2(j = 1)$ for several initial levels of H_2O belonging to the $v_2 = 1, j = 1, 2$ and 3 manifolds. In the middle and lower right panels the opening of excited states (higher in energy than the initial state) of H_2O is also shown. The first reported quantum number on these curves is denoting the rotation of H_2 while the others give the H_2O ro-vibrational state.

Faure and Josselin⁴¹ which includes all H_2O levels below 5000 cm^{-1} and kinetic temperatures up to 5000 K . This dataset is based on literature data combined with a simple extrapolation procedure where rotation and vibration are fully decoupled. Our close-coupling calculations were limited here to water levels $j = 0 - 5$ in the vibrational states (000) and (010) and kinetic temperatures lower than 500 K so that the present dataset as well as that of Wiesenfeld³⁸ are too small for actual astrophysical applications. Calculations will be extended to higher H_2O ro-vibrational levels and higher kinetic temperatures in a future work and the new dataset will be made available in the BASECOL (<https://basecol.vamdc.eu/>) and EMAA databases (<https://emaa.osug.fr/>).

Comparison with experiment : The contributions of p- and o- H_2 are Boltzmann averaged over $j_2=0,1,2$ to obtain the global thermal rate coefficient which is presented in Figure 9, where it is compared to the only experimental data available at 295 K . A first interesting result appears on this figure as contribution of o- H_2 is seen to be negligible below 30 K , but slightly increases with temperature and becomes significant above 100 K . Our computed value at 295 K is $1.18 \times 10^{-12} \text{ cm}^3 \text{ molecule}^{-1} \text{ s}^{-1}$ in excellent agreement with the experimental value of $(1.3 \pm 0.2) \times 10^{-12} \text{ cm}^3 \text{ molecule}^{-1} \text{ s}^{-1}$.

Interestingly, our value is about three times lower than the one obtained for o- H_2O by Wiesenfeld¹⁹ who used a simple direct product of a rigid rotor basis for the rotation and a normal mode function for the vibration. It is however difficult to compare the two kind of calculations which differ in several other aspects. The rotational basis sets both for H_2 and H_2O are different and this author also performed calculations only for selected values of J and interpolated the cross sections for the missing values of J . In order to analyse more clearly the effect of the bending-rotation coupling

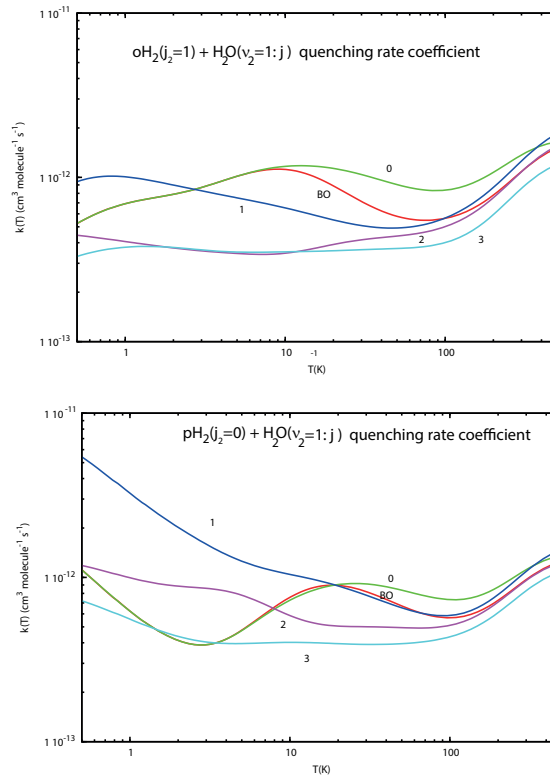


Figure 8: Comparison between the vibrational quenching rate coefficients of the ($v_2 = 1, j = 0, 1, 2$ and 3) states of H_2O by collision with H_2 and the Boltzmann averaged rate coefficient. The collisions with para- H_2 ($j_2 = 0$) and with ortho- H_2 ($j_2 = 1$) are respectively presented in the lower and upper panels.

we then performed new calculations presented in the following paragraph.

Bending-rotation coupling We investigate the effect of the coupling between bending and rotation by performing a new set of calculations neglecting this coupling by using for water a direct product of mono dimensional bending wave function and rigid asymmetric top rotational wave functions while keeping the experimental ordering of the H_2O energies. As we are only interested, in the present study, in the two lowest bending levels of H_2O the coupling with the two stretches can be safely neglected. This approach is very similar to the one used by Wiesenfeld³⁸ which consists in replacing $\Gamma_{v_1'v_2'v_3'}^{j_1'\tau'}$ (R_1, R_2, α) by $\Gamma_{v_1'v_2'v_3'}^{01}$ (R_1, R_2, α) and $\Gamma_{v_1'v_2'v_3'}^{j_1'\tau}$ (R_1, R_2, α) by $\Gamma_{v_1'v_2'v_3'}^{01}$ (R_1, R_2, α) in equation(26).

We represented in the lower panel of Figure 10 the ratio of the present Close Coupling (denoted σ) and approximate state to state cross section (denoted σ^{DP} for direct product) as a function of collision energy for the collisions of p- H_2 with H_2O ($v_2 = 1, 3_{31}$). As can be seen on this figure the ratio of the Close Coupling and approximate state to state cross sections is ranging from 0.4 to 2.2. The coupling is seen not surprisingly to be the strongest for collision energies associated with the region of the well and the long range part of the PES. The strongest peaks which can be seen on this figure are associated with transitions towards the fundamental bending level: p- H_2 ($j_2=4$) + H_2O ($v_2 = 0, 5_{24}$); p- H_2 ($j_2=2$) + H_2O ($v_2 = 0, 5_{42}$); p- H_2 ($j_2=0$) + H_2O ($v_2 = 0, 5_{24}$) and with $\Delta j_2 = 2$. Conversely the strongest bump at very low collision energy is associated with a pure rotational transition inside the excited H_2O bending level towards p- H_2 ($j_2=0$) + H_2O ($v_2 = 1, 3_{22}$).

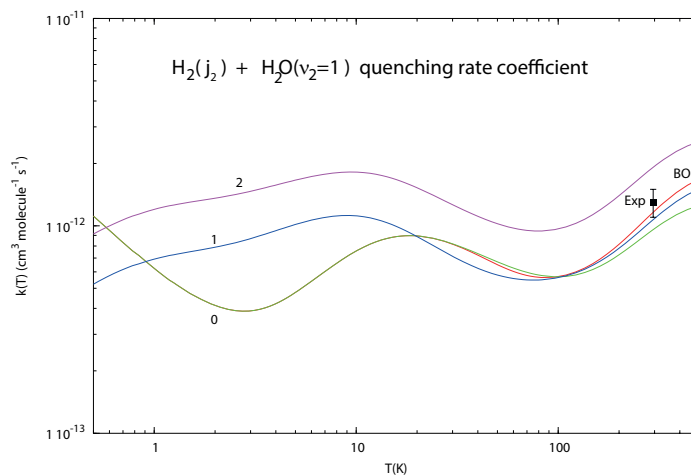


Figure 9: Comparison between the vibrational quenching rate coefficients of H_2O ($v_2 = 1$) by collision with the two spin modifications of H_2 and the global Boltzmann averaged rate coefficient. The only experimental value³⁹ available at 295 K is also reported.

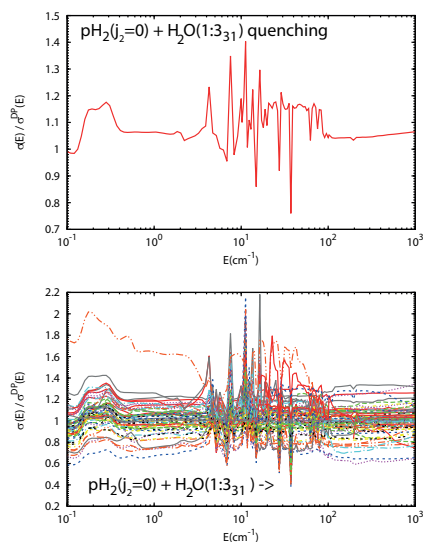


Figure 10: This figure shows the ratio of Close Coupling and direct product state to state cross sections as a function of collision energy for the collisions of p- H_2 with H_2O ($v_2 = 1, 3_{31}$).

If we now examine the ratio of the global bending relaxation cross section of H_2O ($v_2 = 1, 3_{31}$) by collision with p- H_2 ($j=0$) represented in the upper panel of Figure 10 as a function of collision energy we find that the global error is divided by a factor two as the ratio is ranging from 0.7 to 1.4. The curve exhibits a succession of peaks located in the collision energy interval associated with the PES well, demonstrating clearly the resonant character of the coupling between bending and rotation.

CONCLUSION

We presented the first calculations of the bending relaxation of H_2O by collisions with the two spin modifications of H_2 when including exactly the coupling between H_2O bending and rotation. The approach presented also considers the H_2O stretching modes while only the two lowest bending levels were included in the present study. Our approach allowed us to obtain several important results. First, for collision energies associated with the region of the intermolec-

ular potential well, roughly between 10 and 300 K, bending relaxation is controlled by a near-resonant energy transfer mechanism. Consequently, bending relaxation is larger towards the most excited final open rotational level $j_2 = 4$ and decreases monotonously when j_2 decreases for collisions with p-H₂. In the case of collisions with o-H₂ it is the $j_2 = 3$ final channel which is dominating as the $j_2 = 5$ level is closed for several initial levels of the o-H₂ + H₂O($v_2 = 1, jk_A k_C$) system. The Boltzmann weights make furthermore the contribution of the collisions with H₂($j_2 = 1, 2$) negligible at low and moderate temperature. A very good approximation (10% error) of the global bending relaxation rate can be obtained by considering the process to be controlled by the collisions with p-H₂ for the whole interval of temperature of the present study (0.5 – 500 K). Collisions with o-H₂ would do not need in this case to be computed thus dividing computer time by more than a factor of two.

Our computed value of the global bending relaxation rate coefficient at 295 K is in excellent agreement with the experimental value. Future (ideally state-resolved) measurements over an extended range of temperatures will be useful to further test the predictions of the present calculations. We eventually investigated the decoupling between bending and rotation and found that the use of such an approximation leads to error ranging from 50% to 100% respectively for the bending relaxation and state to state cross sections.

ACKNOWLEDGMENTS

This work was supported by the french Agence Nationale de la Recherche (ANR-Waterstars), Contract No. ANR-20-CE31-0011 and by the ECOS-SUD project C22E02. Most of the computer time for this study was provided by the Mésocentre de Calcul Intensif Aquitaine computing facilities of Université de Bordeaux and Université de Pau et des Pays de l'Adour. Part of the computations were performed using the GRICAD infrastructure (<https://gricad.univ-grenoble-alpes.fr>), which is supported by Grenoble research communities.

CONFLICTS OF INTEREST

There is no conflict of interest to report.

REFERENCES

- [1] Cernicharo, J., Agúndez, M., Kahane, C., Guélin, M., Goicoechea, J. R., Marcelino, N., De Beck, E., and Decin, L. Probing the dust formation region in irc +10216 with the high vibrational states of hydrogen cyanide. *Astron. Astrophys.*, 529:L3, 2011.
- [2] J. Cernicharo, J. R. Goicoechea, and E. Caux. *Astrophys. J.*, 580:L199, 2000.
- [3] A. Baudry, K. T. Wong, S. Etoaka, A. M. S. Richards, H. S. P. Muller, F. Herpin, T. Danilovich, M. D. Gray, S. Wallstrom, D. Gobrecht, T. Khouri, L. Decin, C. A. Gottlieb, K. M. Menten, W. Homan, T. J. Millar, M. Montarges, B. Pimpanuwat, J. M. C. Plane, and P. Kervella. *Atomium: Probing the inner wind of evolved o-rich stars with new, highly excited h₂o and oh lines*, 2023.
- [4] G. Perotti, V. Christiaens, Th. Henning, B. Tabone, L. B. F. M. Waters, I. Kamp, G. Olofsson, S. L. Grant, D. Gasman, J. Bouwman, M. Samland, R. Franceschi, E. F. van Dishoeck, K. Schwarz, M. Güdel, P. O. Lagage, T. P. Ray, B. Vandenbussche, A. Abergel, O. Absil, A. M. Arabhavi, I. Argyriou, D. Barrado, A. Boccaletti, A. Caratti o Garatti, V. Geers, A. M. Glauser, K. Justannont, F. Lahuis, M. Mueller, C. Nehmé, E. Pantin, S. Scheithauer, C. Waelkens, R. Guadarrama, H. Jang, J. Kanwar, M. Morales-Calderón, N. Pawellek, D. Rodgers-Lee, J. Schreiber, L. Colina, T. R. Greve, G. Östlin, and G. Wright. *Water in the terrestrial planet-forming zone of the PDS 70 disk*. *Nature*, 620:516–520, July 2023.
- [5] Paul J. Dagdigian and Millard H. Alexander. Theoretical study of the vibrational relaxation of the methyl radical in collisions with helium. *The Journal of Chemical Physics*, 138(10):104317, 2013.
- [6] J. Loreau and A. van der Avoird. Scattering of nh3 and nd3 with rare gas atoms at low collision energy. *The Journal of Chemical Physics*, 143(18):184303, 2015.
- [7] T. Stoecklin, O. Denis-Alpizar, Ph. Halvick, and M.-L. Dubernet. Ro-vibrational relaxation of hcn in collisions with he: Rigid bender treatment of the bending-rotation interaction. *J. Chem. Phys.*, 139:124317, 2013.
- [8] O. Denis-Alpizar, T. Stoecklin, Ph. Halvick, and M.-L. Dubernet. The interaction of he with vibrating hcn: Potential energy surface, bound states, and rotationally inelastic cross section. *J. Chem. Phys.*, 139:034304, 2013.
- [9] MM Al Mogren, O Denis-Alpizar, D Ben Abdallah, T Stoecklin, P Halvick, M-L Senent, and M Hochlaf. On the use of explicitly correlated treatment methods for the generation of accurate polyatomic–he/h2 interaction potential energy surfaces: The case of c3–he complex and generalization. *J. Chem. Phys.*, 141(4):044308, 2014.
- [10] Otoniel Denis-Alpizar, Thierry Stoecklin, and Philippe Halvick. Rovibrational energy transfer in the he-c3 collision: Potential energy surface and bound states. *J. Chem. Phys.*, 140(8):084316, 2014.
- [11] T. Stoecklin, O. Denis-Alpizar, and P. Halvick. Rovibrational energy transfer in the He-C₃ collision: rigid bender treatment of the bending-rotation interaction and rate coefficients. *MNRAS*, 449:3420–3425, June 2015.
- [12] Otoniel Denis-Alpizar, Thierry Stoecklin, and Philippe Halvick. Isotopic effect in the collision of HCN with He: substitution of HCN by DCN. *MNRAS*, 143:114304, 2015.

- [13] Jonathan Tennyson, Maxim A. Kostin, Paolo Barletta, Gregory J. Harris, Oleg L. Polyansky, Jayesh Ramanlal, and Nikolai F. Zobov. Dvr3d: a program suite for the calculation of rotation–vibration spectra of triatomic molecules. *Computer Physics Communications*, 163(2):85 – 116, 2004.
- [14] Thierry Stoecklin, Otoniel Denis-Alpizar, Alexandre Clergerie, Philippe Halvick, Alexandre Faure, and Yohann Scribano. Rigid-bender close-coupling treatment of the inelastic collisions of h₂o with para-h₂. *The Journal of Physical Chemistry A*, 123(27):5704–5712, 2019. PMID: 31192600.
- [15] Dongzheng Yang, Daiqian Xie, and Hua Guo. A time-independent quantum approach to ro-vibrationally inelastic scattering between atoms and triatomic molecules. *The Journal of Physical Chemistry A*, 125(31):6864–6871, 2021. PMID: 34342998.
- [16] Lu Liu, Dongzheng Yang, Hua Guo, and Daiqian Xie. Full-dimensional quantum dynamics studies of ro-vibrationally inelastic scattering of h₂o with ar: A benchmark test of the rigid-rotor approximation. *The Journal of Physical Chemistry A*, 127(1):195–202, 2023. PMID: 36574615.
- [17] Alexandre Faure, Laurent Wiesenfeld, Michael Wernli, and Pierre Valiron. The role of rotation in the vibrational relaxation of water by hydrogen molecules. *The Journal of Chemical Physics*, 123(10):104309, 2005.
- [18] Pierre Valiron, Michael Wernli, Alexandre Faure, Laurent Wiesenfeld, Claire Rist, Stanislav Kedzuch, and Josef Noga. A full nine-dimensional potential-energy surface for hydrogen molecule-water collisions. *Journal of Chemical Physics*, 129:134306, 2008.
- [19] Laurent Wiesenfeld. Quantum nature of molecular vibrational quenching: Water–molecular hydrogen collisions. *The Journal of Chemical Physics*, 155(7), 08 2021. 071104.
- [20] Timothy R. Phillips, Sergio Maluendes, and Sheldon Green. Collision dynamics for an asymmetric top rotor and a linear rotor: Coupled channel formalism and application to H₂O–H₂. *The Journal of Chemical Physics*, 102(15):6024–6031, 04 1995.
- [21] T. R. Phillips, S. Maluendes, and S. Green. Collisional Excitation of H₂O by H₂ Molecules. *The Astrophysical Journal Supplement Series*, 107:467, November 1996.
- [22] Oleg L. Polyansky, Roman I. Ovsyannikov, Aleksandra A. Kyuberis, Lorenzo Lodi, Jonathan Tennyson, and Nikolai F. Zobov. Calculation of rotation-vibration energy levels of the water molecule with near-experimental accuracy based on an ab initio potential energy surface. *The Journal of Physical Chemistry A*, 117(39):9633–9643, 2013. PMID: 23517285.
- [23] Oleg L Polyansky, Aleksandra A Kyuberis, Nikolai F Zobov, Jonathan Tennyson, Sergei N Yurchenko, and Lorenzo Lodi. Exomol molecular line lists xxx : a complete high-accuracy line list for water. *MNRAS*, 2608:2597–2608, 2018.
- [24] Jonathan Tennyson and Brian T. Sutcliffe. Discretization to avoid singularities in vibration–rotation hamiltonians: A bisector embedding for ab₂ triatomics. *International Journal of Quantum Chemistry*, 42(4):941–952, 1992.
- [25] Julián Echave and David C. Clary. Potential optimized discrete variable representation. *Chemical Physics Letters*, 190:225–230, 3 1992.
- [26] Xiao Gang Wang and Tucker Carrington. Using monomer vibrational wavefunctions as contracted basis functions to compute rovibrational levels of an h₂o-atom complex in full dimensionality. *Journal of Chemical Physics*, 146:104105, 3 2017.
- [27] Brian T. Sutcliffe and Jonathan Tennyson. A generalized approach to the calculation of ro-vibrational spectra of triatomic molecules. *Molecular Physics*, 58(6):1053–1066, 1986.
- [28] Viktor Szalay. Discrete variable representations of differential operators. *Journal of Chemical Physics*, 99:1978–1984, 1993.
- [29] Dongzheng Yang, Daiqian Xie, and Hua Guo. A time-independent quantum approach to ro-vibrationally inelastic scattering between atoms and triatomic molecules. *Journal of Physical Chemistry A*, 125:6864–6871, 8 2021.
- [30] T Stoecklin, A Voronin, and JC Rayez. Vibrational quenching of n₋{2}(v=1, j₋{rot}=j) by ³he: Surface and close-coupling calculations at very low energy. *Physical Review A*, 66(4):042703, 2002.
- [31] A. Faure, P. Jankowski, T. Stoecklin, and K. Szalewicz. On the importance of full-dimensionality in low-energy molecular scattering calculations. *Scientific Reports*, 6:28449, June 2016.
- [32] D. E. Manolopoulos. An improved log derivative method for inelastic scattering. *J. Chem. Phys.*, 85(11):6425–6429, 1986.
- [33] Jeremy M. Hutson and Sheldon Green. MOLSCAT: MOlecular SCATtering v. 14. *Astrophysics Source Code Library*, record ascl:1206.004, June 2012.
- [34] Dongzheng Yang, Lu Liu, Daiqian Xie, and Hua Guo. Full-dimensional quantum studies of vibrational energy transfer dynamics between h₂o and ar: theory assessing experiment. *Physical Chemistry Chemical Physics*, 24:13542–13549, 2022.
- [35] Thierry Stoecklin, Lisán David Cabrera-González, Otoniel Denis-Alpizar, and Dayán Páez-Hernández. A close coupling study of the bending relaxation of h₂o by collision with he. *The Journal of Chemical Physics*, 154(14):144307, 2021.
- [36] Daniel, F., Goicoechea, J. R., Cernicharo, J., Dubernet, M.-L., and Faure, A. Influence of collisional rate coefficients on water vapour excitation. *A&A*, 547:A81, 2012.
- [37] K. P. Huber and G Herzberg. *Constants of diatomic molecules*. Springer US, Boston, MA, 1979.
- [38] Laurent Wiesenfeld. Quenching transitions for the rovibrational transitions of water: Ortho-h₂o in collision with ortho- and para-h₂. *The Journal of Chemical Physics*, 157(17), 11 2022. 174304.
- [39] P. F. Zittel and D. E. Masturzo. Vibrational relaxation of h₂o by h₂, hcl, and h₂o at 295 k. *The Journal of Chemical Physics*, 95(11):8005–8012, 1991.
- [40] Alexandre Faure, Pierre Valiron, Michael Wernli, Laurent Wiesenfeld, Claire Rist, Josef Noga, and Jonathan Tennyson. A full nine-dimensional potential-energy surface for hydrogen molecule-water collisions. *Journal of Chemical Physics*, 122:221102, 2005.
- [41] A. Faure and E. Josselin. Collisional excitation of water in warm astrophysical media. I. Rate coefficients for rovibrationally excited states. *A&A*, 492:257–264, December 2008.